Langmuir
Letter
pubs.acs.org/Langmuir

Detection of C-Reactive Protein in Evanescent Wave Field Using Microparticle-Tracking Velocimetry

Yu-Jui Fan,[†] Horn-Jiunn Sheen,*[,†] Yi-Hsing Liu,[‡] Jing-Fa Tsai,[‡] Tzu-Heng Wu,[†] Kuang-Chong Wu,[†] and Shiming Lin[†,§]

[†]*Institute of Applied Mechanics,* [‡]*Engineering Science and Ocean Engineering, and* [§]*Center for Optoelectronic Biomedicine, National Taiwan University, Taipei 106, Taiwan*

Received May 26, 2010. Revised Manuscript Received July 15, 2010

A new technique is developed to measure the nanoparticles' Brownian motions by employing microparticle-tracking velocimetry (micro-PTV) in evanescent wave field, which can provide high signal-to-noise ratio images for analyzing nanoparticles' movements. This method enables real-time detection of C-reactive proteins (CRPs) during the rapid interaction between CRPs and anti-CRP-coated nanobeads as CRP concentrations are related to the nanobeads' Brownian velocity in the equilibrium state. The smallest observable nanobeads with 185 nm were utilized in this experiment to detect CRP concentrations as low as 0.1 μg/mL even in a high-viscosity solution. Further, the dissociation constant, K_D, can be evaluated based on the experimental results.

When light travels from a dense medium (glass with reflective index n_1) into a less dense medium (solution with reflective index n_2), total internal reflection occurs and an evanescent wave propagates along the interface if the incident angle is larger than the critical angle, $\theta_c = \sin^{-1}(n_2/n_1)$. Total internal reflective fluorescence (TIRF) technique, a fluorescence detection method implemented by delivering a laser beam from a thin glass (dense medium) into a sample liquid (less dense medium) to generate an evanescent wave, has proved useful in biological studies, such as cell−substrate contacts,[1] vesicle fusion,[2] and single molecule observation.[3] The images taken under TIRF microscope (TIRFM) have low background noise and clear features of sample structure.[4] Recently, the study of near-wall particle behaviors has become an area of intensive research. TIRF images combined with particle image analysis techniques, such as particle image velocimetry[5] (PIV) and particle tracking velocimetry[4,6] (PTV), were used to experimentally study flow characteristics in the near-surface region. In particular, the Brownian motion of particles traveling in evanescent wave field was carried out based on PTV and TIRF intergration.[7−9]

Brownian motion caused by constant thermal agitation is the random movement of microscopic objects in a fluid, especially significant in the submicrometer scale. Recently, many biosensing issues for antibody−antigen interaction were raised based on the Brownian motion mechanism.[10,11] A multiplex virus detection method was developed through the variation in the Brownian motion of a population of microspheres.[12] Antibody-coated microspheres were tracked in an immunoassay reactor array with different virus concentrations to exactly measure their diffusion coefficients.

In this study, the PTV algorithm for analyzing TIRF images from Brownian motion of nanobeads has been successfully implemented in the quantitative immunosensing aimed at protein-scale molecules. The measurement principle developed to determine the concentration of C-reactive protein (CRP) is schematically given in Scheme 1. Nanobeads (Merck XC010) with a diameter of 185 nm and optimal excitation and emission wavelengths of 475 and 525 nm, respectively, were used in this experiment. Carboxyl functional groups (COOH) modified on the surface of the polystyrene beads were used to conjugate with antibody by following a well-known protocol for efficient two-step coupling using 1-ethyl-3-(3-dimethylaminopropyl) carbodiimide (EDC) and *N*-hydroxysuccinimide (NHS).[13,14] The density of the beads is approximately 1.05 g/cm^3, with negative charge being carried on the surface. First, the cross-linker EDC reacted with carboxyl-coated beads in 2-(*N*-morpholino)ethanesulfonic acid (MES) buffer with a pH value of 5.5. Since EDC is a water-soluble carbodiimide, NHS was used to increase the coupling efficiency. After EDC bound onto the nanobeads, EDC-NHS functionization was used to covalently (NH_2−COOH) link the nanobeads to the antibody (goat anti-human CRP IgG, Sigma C8284). Antibody-coated beads and CRP were mixed and thus injected into a poly(dimethylsiloxane) (PDMS) microchamber, with a depth and diameter of 40 μm and 12 mm, respectively. The reaction was observed through monitoring the Brownian diffusion variations in real-time, illuminated by evanescent wave in the near-wall region. The Brownian motions of the particles were statistically analyzed by micro-PTV. When the antibody-coated nanobeads conjugated with the antigens, the

*To whom correspondence should be addressed. E-mail: sheenh@ntu.edu.tw.

(1) Thompson, P. A.; Troian, S. M. *Nature* **1997**, *389*, 360–362.
(2) Burmeister, J. S.; Olivier, L. A.; Reichert, W. M.; Truskey, G. A. *Biomaterials* **1998**, *19*, 307–325.
(3) Toomre, D.; Manstein, D. J. *Trends Cell Biol.* **2001**, *11*, 298–303.
(4) Jin, S.; Huang, P.; Park, J.; Yoo, J. Y.; Breuer, K. S. *Exp. Fluids* **2004**, *37*, 825–833.
(5) Zettner, C.; Yoda, M. *Exp. Fluids* **2003**, *34*, 115–121.
(6) Huang, P.; Breuer, K. S. *Phys. Fluids* **2007**, *19*, 028104.
(7) Huang, P.; Breuer, K. S. *Phys. Rev. E* **2007**, *76*, 46307.
(8) Choi, C. K.; Margraves, C. H.; Kihm, K. D. *Phys. Fluids* **2007**, *19*, 103305.
(9) Kihm, K. D.; Banerjee, A.; Choi, C. K.; Takagi, T. *Exp. Fluids* **2004**, *37*, 811–824.
(10) Kulin, S.; Kishore, R.; Hubbard, J. B.; Helmerson, K. *Biophys. J.* **2002**, *83*, 1965–1973.
(11) Fan, Y. J.; Sheen, H. J.; Hsu, C. J.; Liu, C. P.; Lin, S.; Wu, K. C. *Biosens. Bioelectron.* **2009**, *25*, 688–694.
(12) Gorti, V. M.; Shang, H.; Wereley, S. T.; Lee, G. U. *Langmuir* **2008**, *24*, 2947–2952.
(13) Cao, Y.; Huang, Z.; Liu, T.; Wang, H.; Zhu, X.; Wang, Z.; Zhao, Y.; Liu, M.; Luo, Q. *Anal. Biochem.* **2006**, *351*, 193–200.
(14) Rocha, S. M.; Suzuki, L. A.; Silva, A. D. T.; Arruda, G. C.; Rossi, C. L. *Rev. Inst. Med. Trop. Sao Paulo* **2002**, *44*, 57–58.

Scheme 1. Schematic Diagram of the Sensing Principle for Measuring the Nanobeads' Brownian Velocities[a]

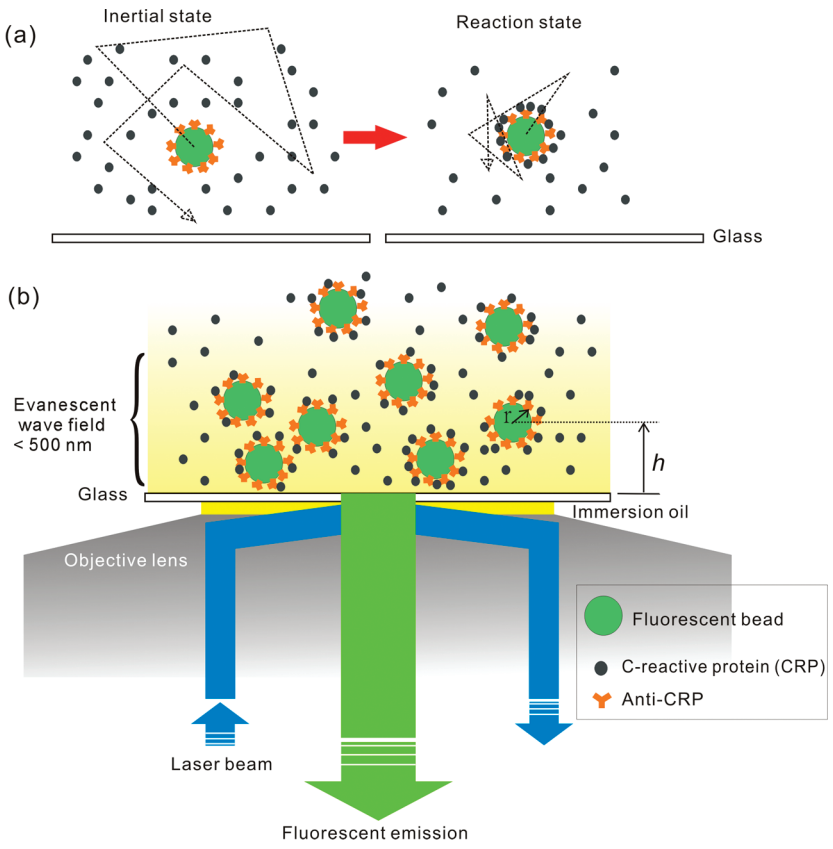

[a] (a) Velocities of antibody-coated nanobeads decrease when antibodies bind with antigens. (b) Objective-based total internal reflective fluorescent microscopy (TIRFM).

nanobeads' diameters increased and their shapes also changed. This phenomenon led to a decrease in the diffusion velocities of the nanobeads.

A TIRF system was used to capture a series of nanobeads' positions in an evanescent wave field in a time period. An inverted microscope (Nikon TE-2000) equipped with a fluorescein isothiocyanate (FITC) filter cube was used to collect the emission lights from the fluorescent nanobeads in epifluorescent mode. The set of FITC filter cube includes an excitation filter, a dichroic mirror, and an emission filter. A 50 mW continuous laser with 473 nm wavelength (Actor Mate) guided by a single-mode fiber was used to generate the evanescent wave at the interface of the glass and the liquid sample. For PTV, the signal-to-noise-ratio (SNR) of the observation plane located in the evanescent wave field can be optimized by adjusting the incident angle of the laser. The dichroic mirror reflected the excitation light while only the emission light could be allowed to transmit. To reduce the background noise, emissions from the fluorescent nanobeads were further filtered by the emission filter. A high-sensitivity CCD (1600 × 1200 pixels) mounted on the microscope was used to receive the fluorescent emissions via an oil-immersed TIRF object lens (Nikon), which had a magnification of 60× and a numerical aperture (NA) of 1.49. A series of TIRF images show high SNR quality even when the size of the fluorescent beads is close to the limit of diffraction ($\sim 0.61\lambda/\mathrm{NA}$, where λ is the wavelength). Each sequence of these images was analyzed by using a PTV algorithm by which the particles were recognized by the first images and their partner images.

Brownian motion, which is a random motion, mainly depends on the particle size, the temperature, and the properties of the solution. The characteristics of Brownian motion were statistically analyzed by Einstein[15] and mathematically described by Langevin.[16] The mean displacement of Brownian motion in one dimension $\langle x \rangle$ is related to the diffusion coefficient D and time intervals Δt as

$$\langle x^2 \rangle = 2D\Delta t \tag{1}$$

where

$$D = \alpha \frac{kT}{3\pi\mu d_p} \tag{2}$$

and $k = 1.3805 \times 10^{-23}$ J/K is the Boltzmann constant, T is the absolute temperature of the fluid, α is the correction factor for boundary effect modification, μ is the dynamic viscosity of the fluid, and d_p is the particle diameter. The parameter x in diffusion coefficient and mean displacement is replaced by velocity, and the mean velocity can be obtained. For a particular solution under isothermal conditions, Brownian velocity depends only on the size of the particle. Equations 1 and 2 indicate that larger particles yield shorter diffusion distances or lower diffusion velocities. The results from Einstein and Langevin show that the mean displacement and mean velocity of the Brownian motion can be described by a Gaussian distribution. The relation between the mean velocity of the Brownian motion and the standard deviation of the particles' velocity distribution (Brownian velocity) V_σ can be

(15) Einstein, A. *Investigations on the Theory of the Brownian Movement*; Dover Publications: New York, 1956.
(16) Langevin, P. *C. R. Acad. Sci.* **1908**, *146*, 530.

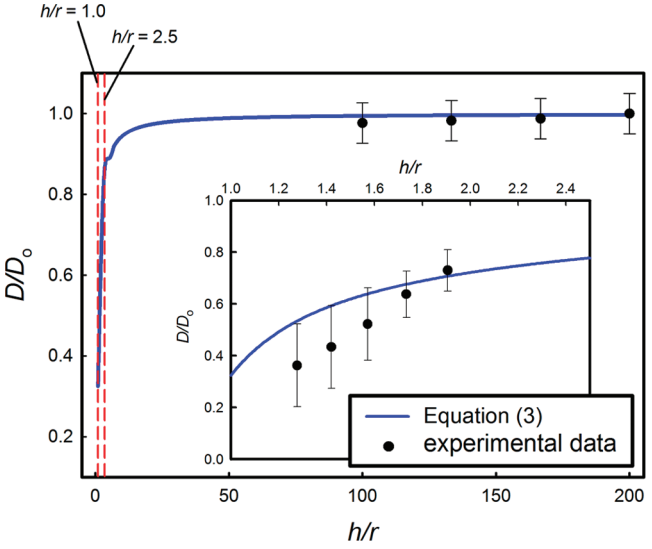

Figure 1. Results of the hindered diffusion coefficient D from the method of reflection, from micro-PTV measurements (main diagram) and from TIRF-enhanced micro-PTV measurements (inset diagram), where D_o is the free diffusion coefficient ($\alpha = 1$) of a nanobead with radius r.

found to be $V_\sigma = (\langle V_p^2 \rangle)^{1/2}$. According to this relationship, the particle velocities of a population of particles, experimentally determined by using micro-PTV, can be used to derive Brownian velocity and diffusion coefficient as well.[11]

In eq 2, $\alpha = 1$ if the suspensions are so dilute that each particle can be regarded as in an infinite fluid field. When the particle is in the vicinity of a solid boundary, its Brownian motion is hindered due to an increase in hydrodynamic drag. The correction factor α should be modified[9] when the distance h, between the geometrical center of the particle and the solid wall, is less than 5 times the particle radius r, as shown in Scheme 1b. The correction factor $\alpha_{||}$ of the near-wall diffusion coefficient in the direction parallel to the boundary surface was given as[17−19]

$$\alpha_{||} = 1 - \frac{9}{16}\left(\frac{h}{r}\right)^{-1} + \frac{1}{8}\left(\frac{h}{r}\right)^{-3} + \frac{45}{256}\left(\frac{h}{r}\right)^{-4} - \frac{1}{16}\left(\frac{h}{r}\right)^{-5} + O\left(\frac{h}{r}\right)^{-6} \quad (3)$$

The above approximation derived from the method of reflection is generally valid for $h/r > 2$. For $h/r \ll 1$, the correction factor can be obtained by an asymptotic solution,[8,20]

$$\alpha_{||} = -\frac{2[\ln(h/r) - 0.9543]}{[(\ln(h/r))^2 - 4.325\ln(h/r) + 1.591]} \quad (4)$$

Figure 1 shows the layer-averaged values of the nanobeads' Brownian diffusion, analyzed by micro-PTV as a function of elevation h, for 185 nm nanobeads in our experiment. The approximation given by eq 3 is also given in the diagram. Although the experimental data for $1 < h/r < 2$ shown in the inset diagram of Figure 1 are outside of the ranges of validity for eq 3, reasonably good agreement can be observed.

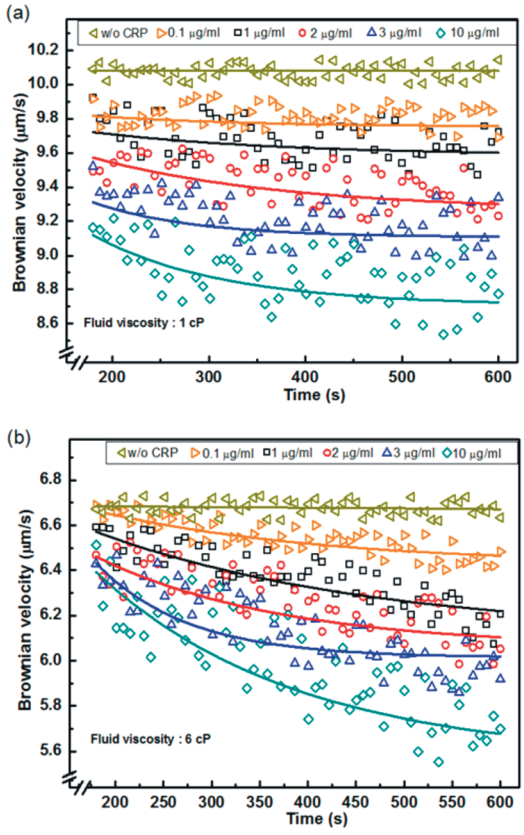

Figure 2. Real-time variations of Brownian velocities for six concentrations (0, 0.1, 1, 2, 3, and 10 μg/mL) of CRPs during the binding processes for 185 nm nanobeads in (a) $\mu = 1$ cP and (b) $\mu = 6$ cP solutions.

The following results were obtained with the observation region around 250 nm away from the glass boundary. The interactions of CRP and anti-CRP by using 185 nm nanobeads with various CRP concentrations, including 0, 0.1, 1, 2, 3, and 10 μg/mL were experimentally investigated. The distributions of Brownian velocities were calculated from the statistical results of every 10-pair images. Moreover, a total of 600 image pairs were acquired and analyzed in a period of 7 min and the variations of the Brownian velocities were thus obtained in real-time.

The results of the real-time variations of Brownian velocities V_σ with respect to different CRP concentrations in viscosity $\mu = 1$ and 6 cP solutions are shown in Figure 2. The transition and the equilibrium states during the antibody-coated nanobeads and CRP reaction can be clearly distinguished from these diagrams. An incubation time of 180 s was required to mix CRP and the nanobeads, to inject the sample into the chamber, and for the fluids to reach static state in macroscopic view. It was found that the binding process of CRPs to the nanobeads, which were conjugated with anti-CRP molecules, led to a decrease of Brownian velocities in the period from 200 to 300 s. The results also indicated that a more dramatic reduction of V_σ could be observed as the concentration of CRPs became higher. From eq 2, one can notice that higher viscosity of the solution leads to lower detection sensitivity. However, in this experiment, a CRP concentration of 0.1 μg/mL in 6 cP glycerin−water solution could be detected.

Due to particle diffraction, when the particle size is less than 300 nm, the SNR of the images becomes too low to be measured by micro-PTV for Brownian motion measurements. However, with TIRF illumination, the Brownian motion behaviors for 185 nm beads can be obtained. The use of smaller beads gives

(17) Happel, J.; Brenner, H. *Low Reynolds number hydrodynamics: With special applications to particulate media*, 2nd ed.; Kluwer Academic: New York, 1983; Chapter 7.
(18) Goldman, A. J.; Cox, R. G.; Brenner, H. *Chem. Eng. Sci.* **1967**, *22*, 637–651.
(19) Lin, B.; Yu, J.; Rice, S. A. *Phys. Rev. E* **2000**, *62*, 3909–3919.
(20) Goldman, A. J.; Cox, R. G.; Brenner, H. *Chem. Eng. Sci.* **1967**, *22*, 653–660.

Table 1. Comparison of Various Microfluidic Device Integrable CRP Sensing Techniques

	detection limitation (mg/L)	process time (min)	fabrication process needed
microantilever beam[21]	1	~10	cantilever and channel
SPR[22]	2−5	30−60 (with assembling time)	gold film and channel
QCM[23]	0.1	N/A	N/A
magnetic bead immunoassay[24]	0.12	~15	channel and magnetic part
Brownian motion Technique (this study)	0.1	~10	chamber

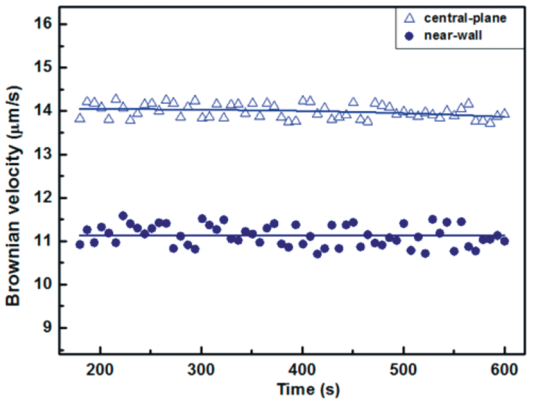

Figure 3. Results of the Brownian velocities at two measurement positions as the bare nanobeads were placed into 10 μg/mL CRP solution.

an advantage that the Brownian velocity variations are larger due to the larger increased volume of the target (antigen) onto the nanobeads. Moreover, the smaller beads have higher Brownian velocity when in aqueous solution. In summary, when measuring smaller nanobeads, this sensing technique can achieve higher sensitivity by using TIRF illumination and micro-PTV.

In this study, this Brownian motion sensing technique can be compactly integrated with microfluidic devices; furthermore, it is a reliable, high sensitivity, short detection time, and MEMS (Micro-Electro-Mechanical-System) fabrication-free technique. Several earlier CRP sensing techniques which can be implemented in microfluidic devices have been reported, including piezoresistive cantilever beam, antibody-coated magnetic particle immunoassay, quartz crystal microbalance (QCM) immunosensor, and surface plasmon resonance (SPR) immunosensor. Table 1 summarizes the characterizations of these CRP sensing techniques.

In order to clarify that the decrease of Brownian velocity did not result from the bare nanobeads and CRP interactions, an additional experiment was carried out. A population of bare nanobeads was placed into a 10 μg/mL CRP solution. The focal planes were at the central and near-wall region of the chamber. The Brownian velocity variations of the bare nanobeads from 180 to 600 s were measured as depicted in Figure 3. The results indicate that there were only small variations in Brownian velocities due to thermal fluctuations and gravitational effects at the two measurement locations.

From Figure 2a, during the reaction processes, the values of the association constant rate k_a and the dissociation constant rate k_d were derived by using kinetic analysis of anti-CRP and CRP interaction in homogeneous solutions. It was assumed that the two epitopes of anti-CRP IgG were equivalent and had no influence on each other. The dissociation constant K_D of CRP−anti-CRP interaction can be determined as $K_D = k_d/k_a$. According to the literature reported by Lin and co-workers,[25,26] the solution can be represented as follows:

$$\frac{d[AgAb]}{dt} = k_a[Ag]\left([Ab]_o - [AgAb]\right) - k_d[AgAb] \qquad (5)$$

where Ag and Ab are antigen and antibody, respectively, [AgAb] is the density of bound analytes, [Ag] is the density of free antigens, and $[Ab]_o$ is the total amount of antibodies on the nanobead surface. In order to obtain the association and dissociation rate constants, eq 5 is rewritten in a form of the variation of R as

$$\frac{dR}{dt} = k_a C R_{max} - (k_a C + k_d)R \qquad (6)$$

where R is [AgAb], C is [Ag], and R_{max} is $[Ab]_o$. In this experiment, C was the concentration of the CRP and R_{max} was the maximum density of combining sites provided on the surface of nanobeads. This equation clearly indicates that a linear relationship exists between dR/dt and R, with a slope $S = -(k_aC + k_d)$. Therefore, k_a and k_d can be evaluated by the linear regression method according to the relationship between the slope S and the concentration C of CRPs. The obtained results of k_a and k_d can then be used to determine the dissociation constant K_D.

From this experiment, k_a and k_d values of the CRP−anti-CRP interaction were found to be $2.71 \times 10^4\ M^{-1}\ s^{-1}$ and $9.70 \times 10^{-3}\ s^{-1}$, respectively, and K_D was estimated to be 3.58×10^{-7} M. Further, from the results in Figure 2b for the μ = 6 cP solution, $K_D = 9.17 \times 10^{-6}$ M was obtained as well. In five determinations, average K_D values of $3.53 \pm 1.4 \times 10^{-7}$ and $9.02 \pm 0.36 \times 10^{-6}$ can be obtained, which were measured in 1 and 6 cP solutions, respectively.

In this study, a novel biosensing technique using micro-PTV combined with TIRF has been successfully developed to measure the antigen−antibody interactions in evanescent wave field. The beads exhibited pronounced volume variation when they were bound with CRPs. Results of the real-time CRP−anti-CRP reactions showed that, during the binding process, the Brownian velocities decreased with time and higher CRP concentration led to lower Brownian velocities in the equilibrium state. Further, the experimental results clearly demonstrated that this new technique has high sensitivity even at a very low concentration of CRP 0.1 μg/mL in glycerin−water solution with a viscosity as high as 6 cP. Based on the relationship between the variations of nanobeads' sizes and CRP concentrations and the kinetic model of the antibody−antigen interaction, the dissociation constant K_D has been evaluated. This Brownian motion measurement technique provides quantitative information for CRP concentrations in real-time. This simple and sensitive sensing technique can be used for quick detection of other biomarkers as well.

Acknowledgment. The authors are grateful for the financial support provided by the National Science Council of Taiwan (NSC 96-2221-E-002-199).

(21) Wee, K.; Kang, G.; Park, J.; Kang, J.; Yoon, D.; Park, J.; Kim, T. *Biosens. Bioelectron.* **2005**, *20*, 1932–1938.
(22) Meyer, M.; Hartmann, M.; Keusgen, M. *Biosens. Bioelectron.* **2006**, *21*, 1987–1990.
(23) Kurosawa, S.; Nakamura, M.; Park, J.; Aizawa, H.; Yamada, K.; Hirata, M. *Biosens. Bioelectron.* **2004**, *20*, 1134–1139.
(24) Tsai, H.; Hsu, C.; Chiu, I.; Fuh, C. *Anal. Chem.* **2007**, *79*, 8416–8419.
(25) Lin, S.; Lee, C. K.; Lin, Y. H.; Lee, S. Y.; Sheu, B. C.; Tsai, J. C.; Hsu, S. M. *Biosens. Bioelectron.* **2006**, *22*, 715–721.
(26) Lin, L.; Huang, L.; Lin, C.; Lee, C.; Chen, J.; Hsu, S.; Lin, S. *Curr. Drug Targets: Immune, Endocr. Metab. Disord.* **2005**, *5*, 61–72.